Available online at www.sciencedirect.com
ScienceDirect
Journal of Sound and Vibration 311 (2008) 554–566
JOURNAL OF SOUND AND VIBRATION
www.elsevier.com/locate/jsvi

Short Communication

Vibration analysis and testing of a thin-walled gradient coil model

Fenglin Wang*, Chris K. Mechefske

Department of Mechanical and Materials Engineering, Queen's University, Kingston, Ontario, Canada K7L 3N6

Received 7 February 2006; received in revised form 20 June 2006; accepted 27 June 2007
Available online 26 November 2007

Abstract

Ongoing development of magnetic resonance imaging (MRI) technology leads to high magnetic field strength (up to 7–9 T) and high-speed switching current in gradient coils for the purpose of improving MRI image quality. These two factors among others contribute largely to the high levels of structure-borne noise that surrounds current MRI scanners. In this paper, the forcing function and distribution acting on gradient coils are described (gradient coils x, y and z). Single point forces and vibration responses of harmonic, transient and impulsive excitations are investigated. Modal expansion method is used to predict the whole cylinder vibration of a thin-walled model under these excitations. Experimental testing of a thin-walled model and a single-layered gradient coil is done by using National Instruments PXI. The measured whole-body radial vibration modes show an agreement with the analytical results. This agreement indicates that modal expansion method could be used to predict the whole-body vibration modes of gradient coils in the low-frequency range.

1. Introduction

Magnetic resonance imaging (MRI) scanners are powerful tools and are used extensively in medical field. However, high levels of structure-borne noise make the diagnostic process extremely uncomfortable. Previous studies by Huwitz et al. [1], Shellock et al. [2], Hedeen et al. [3], have shown that vibration of gradient coils mainly causes the acoustic noise. The gradient coil cylinder in scanning will be acted upon by powerful alternating Lorentz forces, and these dynamic loadings will make the whole-cylinder structure vibrated. Recent studies by Edelstein et al. [4] indicated that the structural vibration will be transformed in complicated manner to other MRI components through mechanical contact. More and more fundamental research has been done by Mechefske et al. [5,6], Yao et al. [7] and Wang et al. [8] in order to uncover the vibration modes of gradient coils and the vibro-acoustic mechanism.

A circular cylinder has long been used as the basic shape of the gradient coil mainly due to the reason that the cylindrical shape is easier to concentrate the uniform magnetic field than others. Physically, a gradient coil is a multiple-layered and thick-walled cylinder structure with different materials, such as the x-coil,

*Corresponding author. Apt. 209, 130 Somerset St. W., Ottawa, ON, Canada K2P 0H9.
Tel.: +1 613 533 3186 (office); fax: +1 613 237 1619 (home).
E-mail addresses: fenglin@me.queensu.ca, fenglin_yan@hotmail.com (F. Wang), chrism@me.queensu.ca (C.K. Mechefske).

0022-460X/$ - see front matter © 2007 Elsevier Ltd. All rights reserved.
doi:10.1016/j.jsv.2007.06.080

y-coil, *z*-coil, imbedded in a plastic cylinder base. Owing to the fact that no theoretical approaches are available to solve thick-walled cylinder dynamics analytically, numerical approaches (finite element methods), as used by Singhal et al. [9] and Yao et al. [10], were utilized in predicting the cylinder complex vibration characteristics. These numerical studies have shown that a large number of complex vibration modes existed in the cylinder dynamic behavior. On the other hand, these numerical results and our experimental studies [8] indicate that the vibration of gradient coil cylinders (thick-walled cylinders) in the low frequency is basically determined by the reference surface, shell thickness, boundary supports, and material properties. Of these features, the reference surface plays a leading role in determining the vibration behavior of the gradient coil cylinder in the low-frequency range (which was demonstrated in our experimental testing). Vibration analyses of the gradient coil based on the thin-walled reference cylinder model are much useful to predict the complicated vibration modes in the low-frequency range and to contribute to the fundamental understanding of the thick-walled gradient coil behavior.

In this paper, vibration of a thin-walled reference cylinder model is analyzed and validated experimentally. Modal participation factors and the mode combination principle are used to investigate the vibration responses of the thin-walled model under different forcing functions. Vibration responses under a point force excitation are described, and the radial vibration modes with corresponding frequencies along the axial length are calculated. The thin-walled reference model and a single-layered gradient coil are further tested by a hammer-exciting system and processed by the ME'scope software. The measured results validate the vibration analysis and prediction.

2. Lorentz forcing function

A schematic of a gradient coil reference cylinder, the isocenter O, and Cartesian/cylindrical coordinate systems are shown in Fig. 1a. In the figure, the gradient winding, carrying the alternating current $I(t)$ on the reference cylinder in a static magnetic field, will be acted on by a point Lorentz force:

$$\mathrm{d}\vec{F}(t,\theta,z) = I(t)(\vec{\alpha}_P \times B_0\,\vec{k})\,\mathrm{d}l, \tag{1}$$

where $\vec{\alpha}_P$ is an unit tangential vector at point P of the gradient winding, $\mathrm{d}l$ is a small arc length along the gradient winding curve, $\mathrm{d}\vec{F}(t,\theta,z)$ is the point Lorentz force acting on the small arc length, B_0 is the magnitude of the static magnet strength in axial direction (the radial strength can be completely neglected).

A unit tangential vector at the point P on the winding curve can be derived from the differential geometry

$$\vec{\alpha}_P = \frac{\mathrm{d}\vec{r}_P}{\mathrm{d}s} = \frac{1}{\sqrt{R^2+\dot{z}^2(\theta)}}[R(-\sin\theta\,\vec{i}+\cos\theta\,\vec{j})+\dot{z}(\theta)\,\vec{k}], \tag{2}$$

where $\vec{r}_P$ is the vector from isocenter to the point P, s is the arc length of the coil curve, R is the radius of the reference cylinder, $\dot{z}(\theta)$ is the coil spatial distribution.

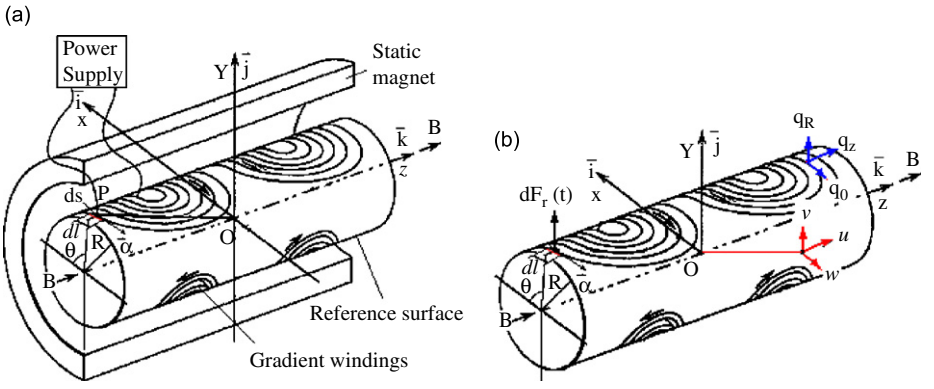

Fig. 1. The schematic of a coordinate setup for the gradient coil system: (a) the gradient coil system; (b) point Lorentz force and response.

Substituting Eq. (2) into Eq. (1) and rewriting the unit tangential vector, the discrete point Lorentz force on the small length of dl can be expressed as

$$\mathrm{d}\vec{F}_r(z,\theta,t) = I(t)\frac{RB_0}{\sqrt{R^2+\dot{z}^2(\theta)}}\,\mathrm{d}l\,\vec{r}, \tag{3}$$

where $\vec{r}$ is an unit vector in radial direction on the reference cylinder.

Eq. (3) shows that the discrete point Lorentz force on the reference cylinder is only in radial direction. Its magnitude is proportional to the alternating current $I(t)$ and the static magnet strength B_0. The point force is also affected by the winding spatial distribution $\dot{z}(\theta)$. Two typical distributions of the point Lorentz forces on gradient coils are shown in Fig. 2. From the figure it can be seen that the forcing function on the gradient x- or y-coil is more complicated than that on the gradient z-coil. So, the structural mobility of the gradient x- or y-coil is more complex than that of the z-coil.

Generally, there are two types of time–frequency forcing functions on gradient coils. One is called "the steady-state excitation", in which the input sequences are steady signals, such as sinusoid signals, trapezoidal signals, and even echo planar imaging (EPI) signals. The vibration response of the steady-state excitation can be described by harmonic analysis. The other type is "the transient-state excitation", in which the inputs are time–frequency signals, such as the impulse excitation and the swept sinusoidal scanning. The transient state vibration responses depend both on time and on the frequency range.

With the development of modern gradient field techniques, a distributed form called "the fingerprint gradient coil" is becoming popular in the gradient winding design. The unwrapped picture of a symmetric

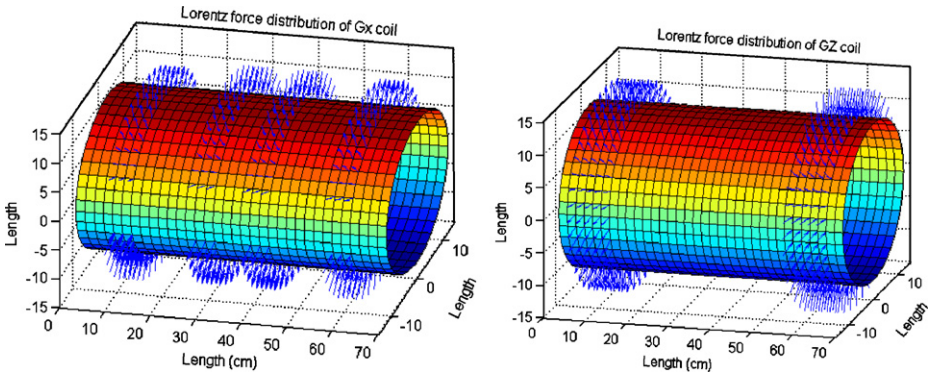

Fig. 2. Lorentz force distributions of the x, y, and z gradient winding.

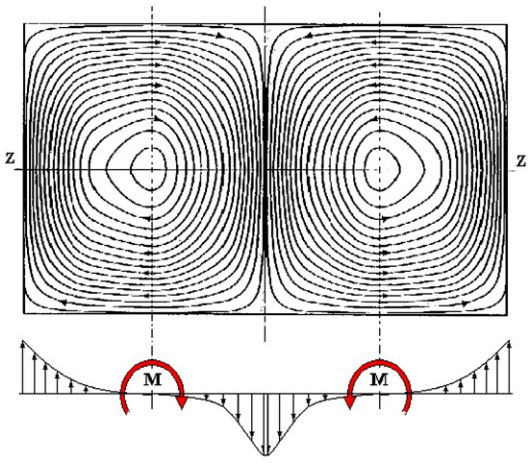

Fig. 3. The equivalent loading of the fingerprint windings.

gradient x "fingerprint" winding is shown in Fig. 3. From this figure it can be seen that the currents flow along spatial curves on the reference cylinder. The winding spatial distribution $\dot{z}(\theta)$ plays an important role in determining the distribution of point Lorentz forces. Applying the principle of Eq. (1) to the winding distribution, two zero-force circles will be formed symmetrically on the coil cylinder and a couple of equivalent bending moments will be formed to bend the cylinder structure.

3. Modal expansion approach

Vibration of a thin-walled reference cylinder can be predicted by using the modal expansion method Soedel [11]. The cylinder displacements can be determined by the sum of a series of orthogonal vectors or modes that satisfy the boundary conditions of the cylinder fixation. As shown in Fig. 1b, the displacements of the thin-walled reference cylinder can be written as:

$$u(z,\theta,t)=\sum_{k=1}^{\infty}\eta_k(t)U_k(z,\theta), \tag{4}$$

$$v(z,\theta,t)=\sum_{k=1}^{\infty}\eta_k(t)V_k(z,\theta), \tag{5}$$

$$w(z,\theta,t)=\sum_{k=1}^{\infty}\eta_k(t)W_k(z,\theta), \tag{6}$$

where $\eta_k(t)$ are modal participation factors in the three displacement directions, $U_k(z,\theta)$, $V_k(z,\theta)$ and $W_k(z,\theta)$ are the natural mode components in the three displacement directions.

Considering the structurally light damping, which is the same values in the three displacement directions, the Love's equations [11] can be written as:

$$L_u\{u,v,w\}-c\frac{\partial u(z,\theta,t)}{\partial t}-\rho h\frac{\partial^2 u(z,\theta,t)}{\partial t^2}=-q_z(z,\theta,t), \tag{7}$$

$$L_v\{u,v,w\}-c\frac{\partial v(z,\theta,t)}{\partial t}-\rho h\frac{\partial^2 v(z,\theta,t)}{\partial t^2}=-q_\theta(z,\theta,t), \tag{8}$$

$$L_w\{u,v,w\}-c\frac{\partial w(z,\theta,t)}{\partial t}-\rho h\frac{\partial^2 w(z,\theta,t)}{\partial t^2}=-q_R(z,\theta,t), \tag{9}$$

where L_u, L_v and L_w are Love's operators, q_z, q_θ and q_R are the force distributions.

Substituting Eqs. (4)–(6) into Eqs. (7)–(9) and integrating the orthogonal series over the thin-walled cylinder [11] give:

$$\frac{\mathrm{d}^2\eta_k(t)}{\mathrm{d}t^2}+\frac{c}{\rho h}\frac{\mathrm{d}\eta_k(t)}{\mathrm{d}t}+\omega_k^2\eta_k(t)=F_k(t), \tag{10}$$

where $F_k(t)$ is the modal force, which can be calculated by

$$F_k(t)=\frac{1}{\rho h D_k}\int_z\int_\theta[q_z(z,\theta,t)U_k+q_\theta(z,\theta,t)V_k+q_R(z,\theta,t)W_k]R\,\mathrm{d}z\,\mathrm{d}\theta, \tag{11}$$

$$D_k=\int_z\int_\theta(U_k^2+V_k^2+W_k^2)R\,\mathrm{d}z\,\mathrm{d}\theta. \tag{12}$$

4. Vibrations of the thin-walled model

4.1. Steady-state harmonic response

A single-pointed radial force is the basic loading characteristic of the gradient coil cylinder. According to Saint-venant's principle, although the deformation near the force point is violated, the deformations outside the point or on the whole coil cylinder would be valid. For the point Lorentz force at the point P, the force distributions are:

$$q_z(z,\theta,t)=0, \tag{13}$$

$$q_\theta(z,\theta,t)=0, \tag{14}$$

$$q_R(z,\theta,t)=\frac{\mathrm{d}F_r(z,\theta,t)}{R}\delta(z-z^j)\delta(\theta-\theta^j), \tag{15}$$

where z^j and θ^j are the coordinates of the point force $\mathrm{d}F_r(z,\theta)$, $\delta(\cdot)$is the Dirac delta function and is defined as:

$$\delta(z-z^j)=0 \ \ (\text{if } z\neq z^j) \text{ and } \int_{t=-\infty}^{t=\infty}\delta(z-z^j)\,\mathrm{d}t=1 \ (\text{if } z=z^j),$$

$$\delta(\theta-\theta^j)=0 \ (\text{if } \theta\neq\theta^j) \ \text{ and } \int_{t=-\infty}^{t=\infty}\delta(\theta-\theta^j)\,\mathrm{d}t=1 \ (\text{if } \theta\neq\theta^j).$$

For the simply supported boundary condition and a harmonic current $I(t)=\sin(\omega t)$, the modal force $F_k^j(t)$ is

$$F_k^j(t)=\frac{\mathrm{d}F_r(z^j,\theta^j)\sin(\omega t)}{\rho h D_{mni}}\sin\left(\frac{m\pi z^j}{L}\right)\cos[n(\theta-\theta^j)], \tag{16}$$

where

$$D_{mni}=\begin{cases}\left[\left(\dfrac{U_{mni}}{W_{mni}}\right)^2+\left(\dfrac{V_{mni}}{W_{mni}}\right)^2+1\right]\dfrac{LR\pi}{2} & \text{if } n\neq 0,\\ \left[\left(\dfrac{U_{mni}}{W_{mni}}\right)^2+1\right]LR\pi & \text{if } n=0.\end{cases}$$

The cylinder harmonic displacements under the point force $\mathrm{d}F_r(z^j,\theta^j)$ excitation are:

$$u_{z^j,\theta^j}(z,\theta,t)=\sum_i^{z,\theta,R}\sum_{m=1}^{\infty}\sum_{n=0}^{\infty}\frac{U_{mni}}{W_{mni}}\frac{\mathrm{d}F_r(z^j,\theta^j)\sin(m\pi z^j/L)\cos[n(\theta-\theta^j)]\cos(m\pi z/L)}{\rho h D_{mni}\omega_{mni}^2\sqrt{[1-(\omega/\omega_{mni})^2]^2+4\zeta_{mni}^2(\omega/\omega_{mni})^2}}\sin(\omega t-\phi_{mni}), \tag{17}$$

$$v_{z^j,\theta^j}(z,\theta,t)=\sum_i^{z,\theta,R}\sum_{m=1}^{\infty}\sum_{n=0}^{\infty}\frac{V_{mni}}{W_{mni}}\frac{\mathrm{d}F_r(z^j,\theta^j)\sin(m\pi z^j/L)\sin[n(\theta-\theta^j)]\sin(m\pi z/L)}{\rho h D_{mni}\omega_{mni}^2\sqrt{[1-(\omega/\omega_{mni})^2]^2+4\zeta_{mni}^2(\omega/\omega_{mni})^2}}\sin(\omega t-\phi_{mni}), \tag{18}$$

$$w_{z^j,\theta^j}(z,\theta,t)=\sum_i^{z,\theta,R}\sum_{m=1}^{\infty}\sum_{n=0}^{\infty}\frac{\mathrm{d}F_r(z^j,\theta^j)\sin(m\pi z^j/L)\cos[n(\theta-\theta^j)]\sin(m\pi z/L)}{\rho h D_{mni}\omega_{mni}^2\sqrt{[1-(\omega/\omega_{mni})^2]^2+4\zeta_{mni}^2(\omega/\omega_{mni})^2}}\sin(\omega t-\phi_{mni}), \tag{19}$$

where

$$\zeta_{mni}=\frac{c}{2\rho h\omega_k},\quad \phi_{mni}=\tan^{-1}\frac{2\zeta_{mni}(\omega/\omega_{mni})}{1-(\omega/\omega_{mni})^2}.$$

4.2. Transient-state vibration responses

4.2.1. Swept sinusoidal excitation

A swept sinusoidal signal or a chirp signal contains both time and frequency information, and has been a typical signal used in structure modal testing. In order to get the accurate frequency response function (FRF), the swept progress through the interested frequency band has to be slow enough to allow the gradient coil response to persist for measurements to be taken [12]. Among different time–frequency swept processes, a linear chirp signal with constant amplitude and linearly increasing frequency with respect to time gives the best signal-to-noise ratio excitation. The linear chirp signal can be expressed as

$$S_j(t) = S_0 \sin \theta_S = S_0 \sin\left(\omega_0 t + \frac{1}{2}\beta t^2\right) = S_0 \sin\left[2\pi f_0 + \pi\left(\frac{f_1 - f_0}{t_S}\right)t^2\right], \tag{20}$$

where S_0 is the constant amplitude, θ_S is the total angular rotation, ω_0 is the starting angular velocity with starting frequency f_0, t_S is the swept time interval, β is the constant value of angular acceleration.

For a point loading $S_j(t)$ of the linear chirp excitation, Eq. (15) becomes:

$$q_R(z,\theta,t) = \frac{S_j(t)}{R}\delta(z - z^j)\delta(\theta - \theta^j). \tag{21}$$

Under zero-initial condition, the modal force can be expressed as

$$S_k^j(t) = \frac{S_j(t)}{\rho h D_{mni}} \sin\left(\frac{m\pi z^j}{L}\right) \cos[n(\theta - \theta^j)]. \tag{22}$$

The cylinder vibration responses are:

$$u_{z^j,\theta^j}(z,\theta,t) = \sum_i^{z,\theta,R} \sum_{m=1}^{\infty} \sum_{n=0}^{\infty} \frac{U_{mni}}{W_{mni}} \frac{\sin(m\pi z^j/L)\cos[n(\theta - \theta^j)]\cos(m\pi z/L)}{\rho h D_{mni}\omega_{mni}\sqrt{1-\zeta_{mn}^2}} \int_0^t S^j(\tau) e^{-\zeta_{mn}\omega_{mni}(t-\tau)} \sin\left[\omega_{mni}\sqrt{1-\zeta_{mn}^2}(t-\tau)\right] d\tau, \tag{23}$$

$$v_{z^j,\theta^j}(z,\theta,t) = \sum_i^{z,\theta,R} \sum_{m=1}^{\infty} \sum_{n=0}^{\infty} \frac{V_{mni}}{W_{mni}} \frac{\sin(m\pi z^j/L)\sin[n(\theta - \theta^j)]sin(m\pi z/L)}{\rho h D_{mni}\omega_{mni}\sqrt{1-\zeta_{mn}^2}} \int_0^t S^j(\tau)\, e^{-\zeta_{mn}\omega_{mni}(t-\tau)} \sin\left[\omega_{mni}\sqrt{1-\zeta_{mn}^2}(t-\tau)\right] d\tau, \tag{24}$$

$$w_{z^j,\theta^j}(z,\theta,t) = \sum_i^{z,\theta,R} \sum_{m=1}^{\infty} \sum_{n=0}^{\infty} \frac{\sin(m\pi z^j/L)\cos[n(\theta - \theta^j)]\,\sin(m\pi z/L)}{\rho h D_{mni}\omega_{mni}\sqrt{1-\zeta_{mn}^2}} \int_0^t S^j(\tau) e^{-\zeta_{mn}\omega_{mni}(t-\tau)} \sin\left[\omega_{mni}\sqrt{1-\zeta_{mn}^2}(t-\tau)\right] d\tau. \tag{25}$$

4.2.2. Hammer excitation

An impulse loading is also used in modal testing experiments and the impulse magnitude P is concentrated in a very short period of time. Eq. (15) can be expressed as

$$q_R(z,\theta,t) = \frac{P\delta(t - t_1)}{R}\delta(z - z^j)\delta(\theta - \theta^j). \tag{26}$$

Under the zero-initial condition, the modal force becomes

$$P_k^j(t) = \frac{P}{\rho h D_{mni}} \sin\left(\frac{m\pi z^j}{L}\right) \cos[n(\theta - \theta^j)]. \tag{27}$$

Cylinder displacements under the impulse point excitation can be written as:

$$u_{z^j,\theta^j}(z,\theta,t) = \sum_{i=1}^{z,\theta,R}\sum_{m=1}^{\infty}\sum_{n=0}^{\infty}\frac{U_{mni}}{W_{mni}}\frac{P\sin(m\pi z^j/L)\cos[n(\theta-\theta^j)]\cos(m\pi z/L)}{\rho h D_{mni}\omega_{mni}\sqrt{1-\zeta_{mni}^2}} \mathrm{e}^{-\zeta_{mn}\omega_{mni}(t-t_1)}\sin\left[\omega_{mni}\sqrt{1-\zeta_{mni}^2}(t-t_1)\right]\mathrm{d}\tau, \tag{28}$$

$$v_{z^j,\theta^j}(z,\theta,t) = \sum_{i}^{z,\theta,R}\sum_{m=1}^{\infty}\sum_{n=0}^{\infty}\frac{V_{mni}}{W_{mni}}\frac{P\sin(m\pi z^j/L)\sin[n(\theta-\theta^j)]\sin(m\pi z/L)}{\rho h D_{mni}\omega_{mni}\sqrt{1-\zeta_{mni}^2}} \mathrm{e}^{-\zeta_{mn}\omega_{mni}(t-t_1)}\sin\left[\omega_{mni}\sqrt{1-\zeta_{mni}^2}(t-t_1)\right]\mathrm{d}\tau, \tag{29}$$

$$w_{z^j,\theta^j}(z,\theta,t) = \sum_{i}^{z,\theta,R}\sum_{m=1}^{\infty}\sum_{n=0}^{\infty}\frac{P\sin(m\pi z^j/L)\cos[n(\theta-\theta^j)]\sin(m\pi z/L)}{\rho h D_{mni}\omega_{mni}\sqrt{1-\zeta_{mni}^2}} \mathrm{e}^{-\zeta_{mn}\omega_{mni}(t-t_1)}\sin\left[\omega_{mni}\sqrt{1-\zeta_{mni}^2}(t-t_1)\right]\mathrm{d}\tau. \tag{30}$$

4.3. Calculation results

Vibration mode calculation of a thin-walled cylinder is carried out based on the geometrical parameters and material properties listed in Table 1. In the calculation, three types of cylindrical modes-bending modes, torsional modes, and axial modes are added to contribute their modal participation factors to the displacement responses. The structural damping ratio is chosen as a constant of 0.018 as we measured before. The impulse excitation force is applied to the middle of the thin-walled cylinder with the simply supported boundary condition. This intending location will excite the odd beam-vibration patterns of the thin-walled cylinder and will make a comparison with experimental measurement results.

The displacement responses of the cylinder model at the low frequencies of 243, 391, 610, 735, 882, and 1105 Hz are shown in Fig. 4. In the calculation the modal expansion order of 16 was used. From the Figure it can be seen that the fundamental odd simply supported beam modes are the main deformation shapes. Upon the beam vibration patterns, ring vibration patterns are superimposed in regular linear combinations. The vibration modes presented are similar to the bending modes but with different modal participation factors.

The amplitude–frequency analysis of the thin-walled cylinder for a wide-frequency range is calculated as well to reveal the modal density along the cylinder length. A modal expansion order of 20 is used to predict the displacement responses along the length of the cylinder. The frequency ranges are from 500 to 2500 Hz and the displacement responses as shown in Fig. 5 are virtually "measured" along the axial length. From the figures it can be seen that in the low-frequency range the beam-patterns up to the third mode are the main modal components. But in the high-frequency range there exist a high modal density of beam-patterns up to the fifth order, which make the dynamic responses of the thin-walled cylinder complex.

Table 1
Parameters of the thin-walled reference cylinder model

Length (L)	590 mm
Radius (R)	187.75 mm
Thickness (h)	11.5 mm
Geometric ratio (R/h)	16.3
Young's modulus (E)	2.8×10^9 Pa
Poisson's ratio (v)	0.39
Mass density (ρ)	1200 kg m^{-3}

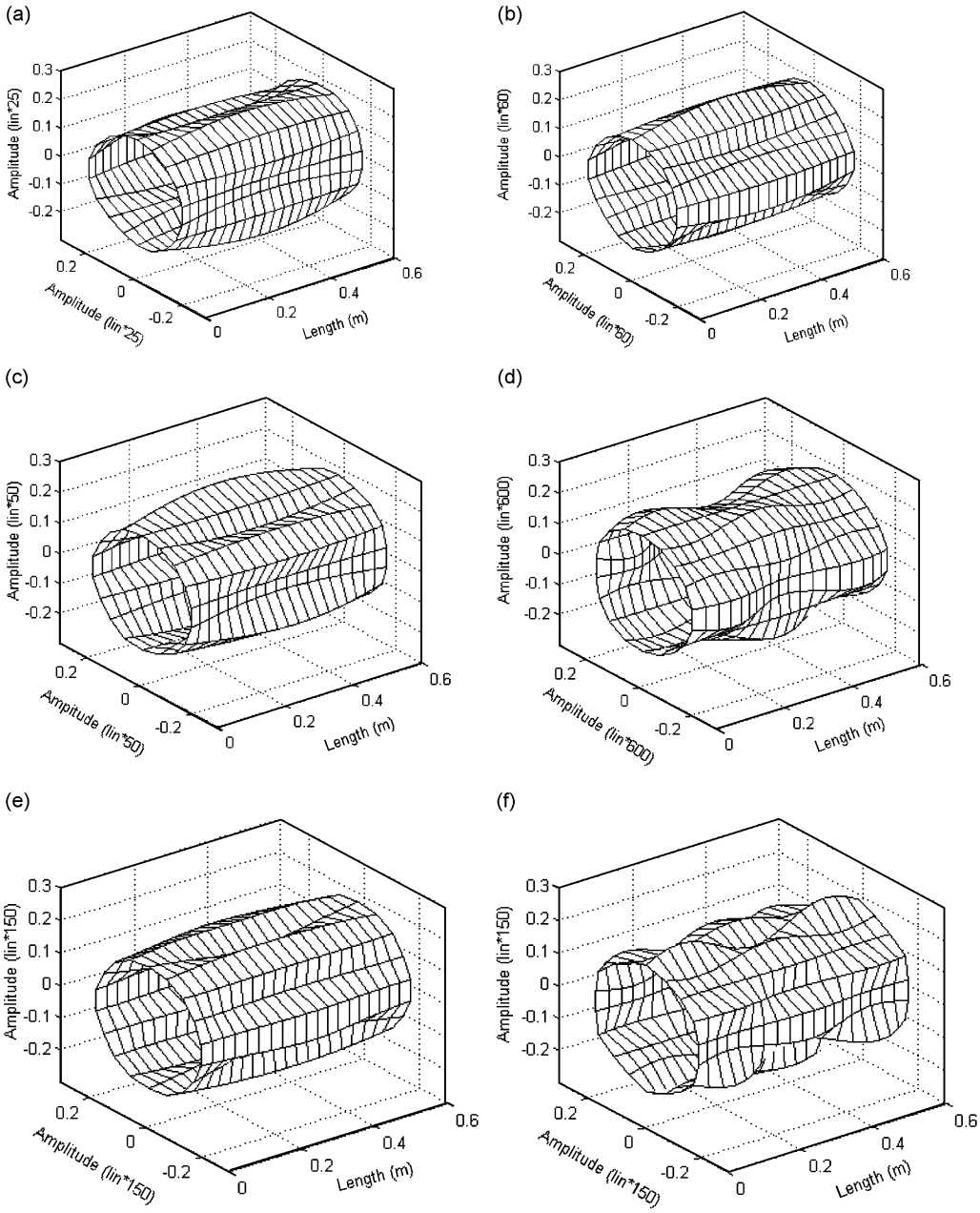

Fig. 4. The vibration responses of the thin-walled model at the low frequencies.

5. Experimental verification and testing

The vibration testing system for gradient coil models was designed by using the National Instruments (NI) PXI 1020 together with a series of micro-accelerometers, signal conditioners and an impact hammer. In the system, a digital spectrum analyzer was programmed in LabVIEW system. To get the vibration modes of whole cylinder models, hundreds of measuring points were evenly distributed on the testing cylinder surface. Two gradient coil cylinders were tested: one is the thin-walled reference cylinder as shown in Fig. 6a and the other is a single-layered gradient x-coil as shown in Fig. 6b. For the thin-walled cylinder, both ends were fastened to thin-wall aluminum plates supported by two steel columns. This kind of installation is meant to

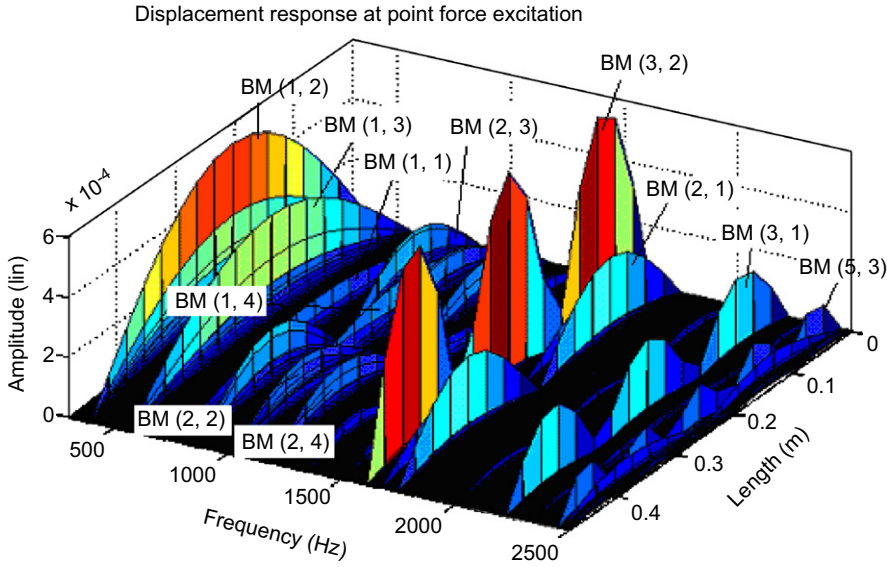

Fig. 5. The amplitude–frequency response in the frequency from 500 to 2500 Hz.

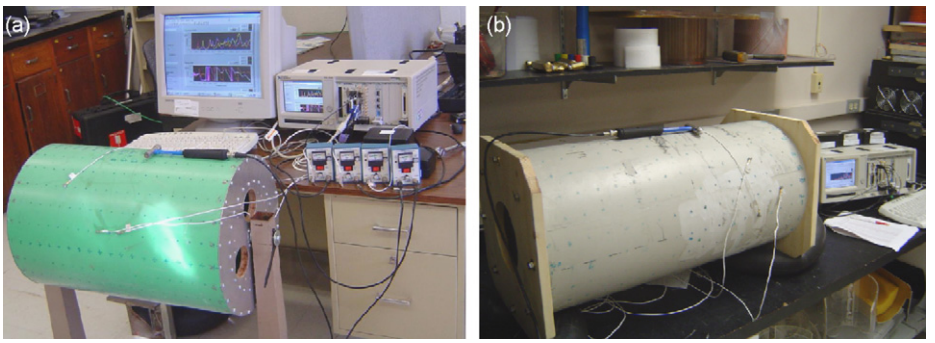

Fig. 6. Experimental setup for the thin-walled model and a gradient coil.

simulate the installation condition of gradient coils in a 4T MRI scanner. This installing condition can be considered as the simply supported boundary condition. For a single-layered gradient coil, both ends were fixed to wooden plates by 6 evenly distributed screws, which can be regarded as the clamp-clamp boundary condition or close to the simply supported boundary condition. The geometrical parameters and material properties of the single-layered gradient coil are listed in Table 2.

In order to compare with the simulated vibration modes, the impact hammer was used to excite a point in the middle of the gradient coil models, and the odd-numbered axial modes were excited. At each measuring point, FRF was measured by using the digital spectrum analyzer. The FRFs of these measuring points were collected and processed by ME'scope software. The vibration modes and the corresponding frequencies of the two cylinders are extracted and shown in Figs. 7 and 8, respectively. In Fig. 7, it can be seen that the comparison between the measured vibration modes and the vibration responses predictions in Fig. 4 matches quite well.

Fig. 8 shows the tested vibration modes of the single-layered gradient coil. Compared to Fig. 7, the measured natural frequencies are much higher than those of the thin-walled cylinder. This may be due to the fact that its Young's modulus, its geometric ratio of length over radius, and cylinder boundary conditions are much different from those of the thin-walled cylinder. However, it can be seen that there is a good agreement in the vibration modes between the single-layered gradient coil and the thin-walled reference cylinder. Most vibration modes of the single-layered gradient coil are very similar to the counter parts of the

Table 2
Parameters of a single-layered gradient coil

Length (L)	700 mm
Radius (R)	165 mm
Thickness (h)	20 mm
Geometric ratio (R/h)	8.25
Young's modulus (E)	$31{,}030 \times 10^6$ Pa
Poisson's ratio (v)	0.32
Mass density (ρ)	2241.4 kg m^{-3}

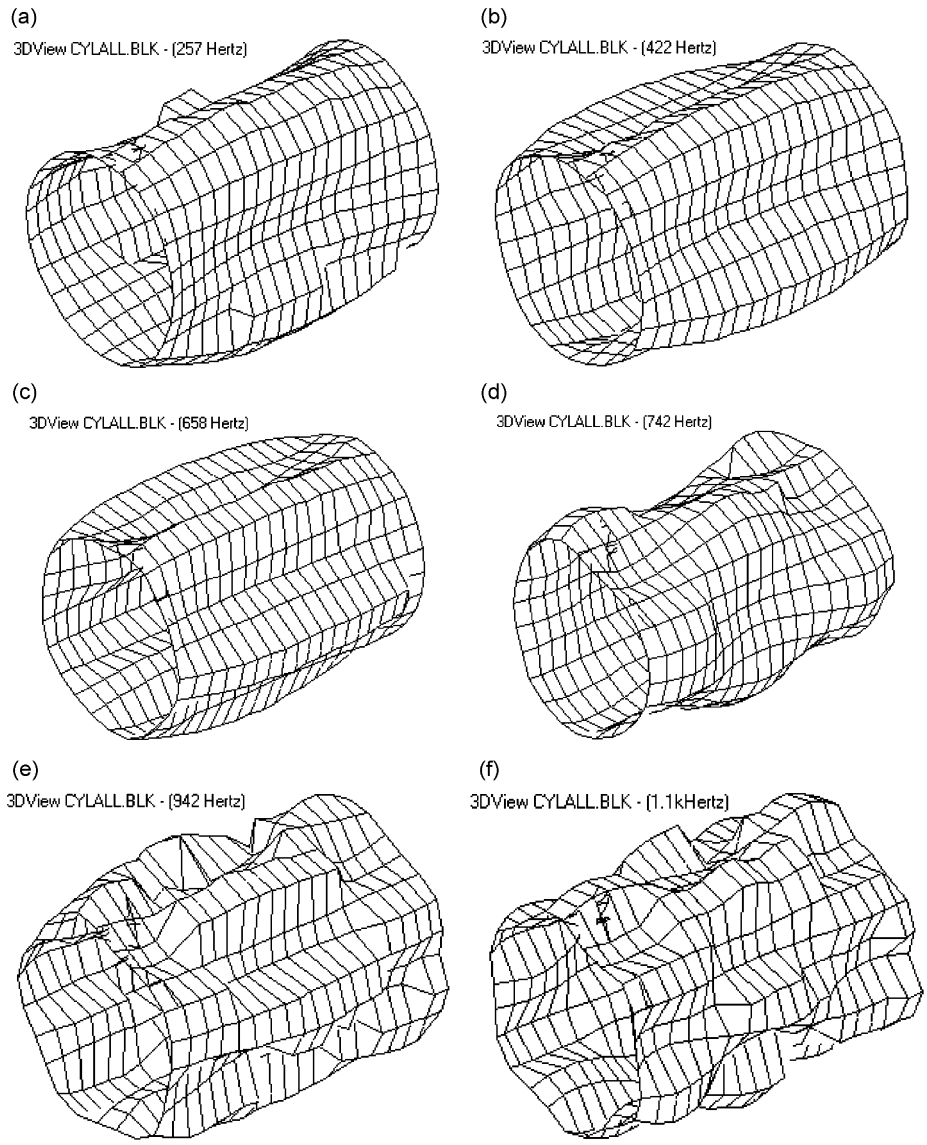

Fig. 7. The vibration modes of the thin-walled model under the impact excitation: (a) vibration response at 257 Hz; (b)vibration response at 422 Hz; (c) vibration response at 658 Hz; (d) vibration response at 742 Hz; (e) vibration response at 942 Hz; and (f) vibration response at 1167 Hz.

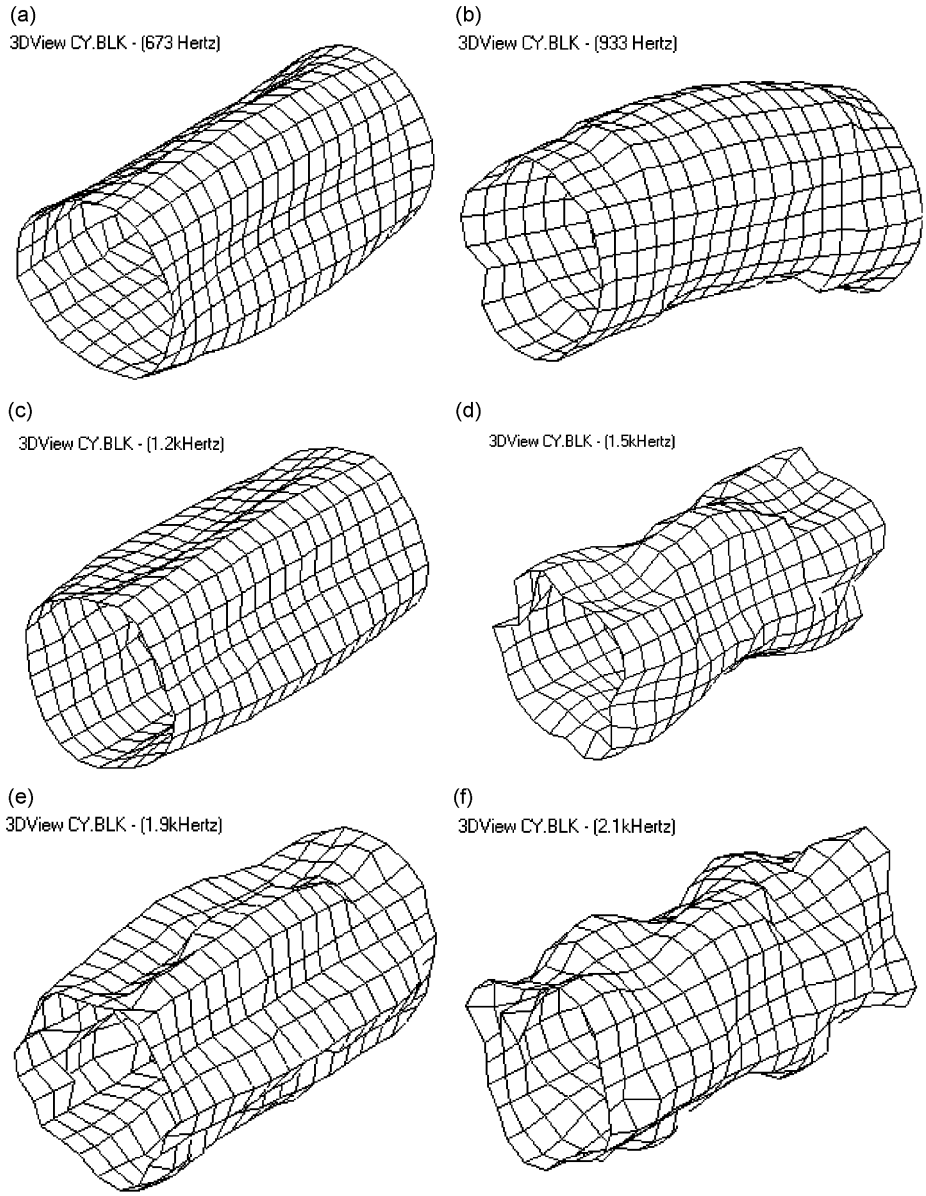

Fig. 8. The vibration modes of a single-layered gradient coil under impact excitations: (a) vibration response at 673 Hz; (b) vibration response at 933 Hz; (c) vibration response at 1244 Hz; (d) vibration response at 1497 Hz; (e) vibration response at 1934 Hz; and (f) vibration response at 2124 Hz.

thin-walled model except for the 993 Hz mode in the thin-walled model and the 422 Hz mode in the single-layered gradient coil. The probable reason might be the different material properties and geometric shapes. The experimental vibration results sufficiently verify the thin-walled cylinder model could be used to predict the vibration modes of the non-thin-walled gradient coil in the low-frequency range although there are errors in the natural frequency prediction.

6. Conclusions

It has long been known that MRI acoustic problems mainly come from the vibration of gradient coils in scanning. Owing to the structural complexity and the thick-walled cylinder with multi-layered different

materials, analytical analysis and prediction of the gradient coil vibration in scanning become very difficult. Based on our experimental testing, the dynamic behavior of gradient coils is basically determined by the cylinder reference surface, the cylinder thickness, the cylinder supports, and the cylinder materials. In the low-frequency range the cylinder reference surface is the most significant. In the paper, a thin-walled cylinder model and its vibration prediction under different excitation cases are investigated. Some conclusions on the dynamic analysis of gradient coils can be drawn as follows:

(1) The forcing functions of gradient coils are characterized by the discrete point Lorentz forces distributed on a reference cylinder. These point forces are only in the radial directions changing with the different time–frequency features which are determined by the scanning current waveforms. The structural mobility of gradient x or y-coil is higher than that of gradient z-coil. The magnitude of forcing functions are not only determined by the current and the magnetic strength, but also affected by the coil spatial distribution;
(2) In the low-frequency range, the vibration modes of the gradient coil cylinder might be predicted by using a thin-walled cylinder model with the point force excitation. Modal expansion methods can be applied to analytically simulate the vibration responses to various types of point Lorentz forces including the harmonic, swept sinusoidal and impulse excitations;
(3) Experimental validation of a thin-walled cylinder vibration modes and testing of a single-layered gradient coil were performed by using a modal testing system, which is extremely important for future study and testing of multi-layered gradient coil system;
(4) In the low frequency, finding a thin-walled cylinder model matching to the vibration behavior of a real single-layered gradient coil is our next research. The measured vibration modes of the single-layered gradient coil are basically composed of the beam-vibration patterns with corresponding boundary condition linearly superimposed by the ring vibration patterns.

Acknowledgments

Financial support for this work was provided by the Natural Sciences and Engineering Research Council of Canada (NSERC) and the Canadian Institutes for Health Research (CIHR).

Appendix A. Supplementary materials

Supplementary data associated with this article can be found in the online version at doi:10.1016/j.jsv.2007.06.080

References

[1] R. Huwitz, S.R. Lane, R.A. Bell, M.N. Brant-Zawadzki, Acoustic analysis of gradient coil noise in MR imaging, *Radiology* 173 (1989) 545–548.
[2] F.G. Shellock, S.M. Morisoli, M. Ziarati, Measurement of acoustic noise during MR imaging: evaluation of six "worst-case" pulse sequences, *Radiology* 191 (1994) 91–93.
[3] R.A. Hedeen, W.A. Edelstein, Characterization and prediction of gradient acoustic noise in MRI imaging, *Magnetic Resonance in Medicine* 37 (1997) 7–10.
[4] W.A. Edelstein, R.A. Hedeen, R.P. Mallozzi, S.A. El-Hamamsy, R.A. Ackermann, T.J. Havens, Making MRI quieter, *Magnetic Resonance Imaging* 20 (2002) 155–163.
[5] C.K. Mechefske, G. Yao, F.L. Wang, Vibration and acoustic noise characterization of a gradient coil insert in a 4 T MRI, *Journal of Vibration and Control* 10 (2004) 861–880.
[6] C.K. Mechefske, G. Yao, W. Li, C. Gazdzinski, B.K. Rutt, Modal analysis and acoustic noise characterization of a 4 T MRI gradient coil insert, *Concepts in Magnetic Resonance, Part B: Magnetic Resonance Engineering* V22B (2004) 37–49.
[7] G.Z. Yao, C.K. Mechefske, F.L. Wang, B.K. Rutt, Modal analysis of a gradient coil insert for a 4 T MRI scanner, *The International Society of Magnetic Resonance in Medicine Conference*, Toronto, Canada, May 12–16, 2003.
[8] F.L. Wang, C.K. Mechefske, Modal analysis and testing of the thin-walled gradient cylinder model, *Concepts in Magnetic Resonance, Part B: Magnetic Resonance Engineering* 27B (2005) 34–50.

[9] R.K. Singhal, W. Guan, K. Williams, Modal analysis of a thick-walled circular cylinder, *Mechanical System and Signal Processing* V16 (2002) 141–153.
[10] G. Yao, C.K. Mechefske, B.K. Rutt, Characterization of vibration and acoustic noise in a gradient-coil insert, *MAGMA—Magnetic Resonance Materials in Physics, Biology and Medicine* V17 (2004) 12–27.
[11] W. Soedel, *Vibrations of Shells and Plates*, third ed., Marcel Deckker Inc., New York, 2004.
[12] D.J. Ewins, *Modal Testing: Theory, Practice and Application*, second ed., Research Studies Press Ltd., England, 2000.